Journal of Materials Chemistry A

Accepted Manuscript

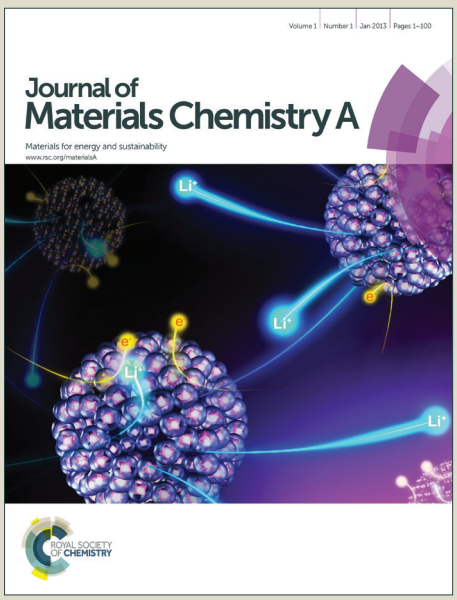

ROYAL SOCIETY OF CHEMISTRY

www.rsc.org/materialsA

Journal Name

RSCPublishing

COMMUNICATION

High Performance Hybrid Asymmetric Supercapacitor via Nano-scale Morphology Control of Graphene, Conducting Polymer, and Carbon Nanotube Electrodes

Cite this: DOI: 10.1039/xoxxoooooox

Received ooth January 2012,
Accepted ooth January 2012

DOI: 10.1039/xoxxoooooox

www.rsc.org/

Yue Zhou,[a] Noa Lachman,[b] Mehdi Ghaffari,[c] Haiping Xu,[a,d] Dhiman Bhattacharya,[e] Pouria Fattahi,[f] Mohammad Reza Abidian,[f] Shan Wu,[a] Karen K. Gleason,[e] Brian L. Wardle,[b]* and Q. M. Zhanga[a,c]*

An asymmetric supercapacitor, exploiting an ultra-high density aligned activated graphene flakes as the positive electrode, and nm-scale conformal coating of a conducting polymer, poly(ethylenedioxythiophene) on aligned carbon nanotubes as the negative electrode, is introduced. By complementary tailoring of the asymmetric electrodes, the layered device exhibits a wide 4V electrochemical window, with the highest power density (149 kW L^{-1}) and energy density (113 Wh L^{-1}) reported thus far for carbon-based supercapacitors.

Supercapacitors are promising energy storage devices due to their higher energy density than dielectric capacitors and higher power density and long cycle life time (> millions) compared with conventional batteries.[1-4] In order to meet the demands of a wide range of energy technologies, such as hybrid electric vehicles, backup power sources and portable electronic equipment, supercapacitors with higher energy (and power) densities are required.[1,5-9] In the past decade a large number of ideas have sought to improve upon state-of-art supercapacitors comprised of activated carbon powders, including employing carbon nanotubes and graphene as the active materials.[7, 10, 11] For supercapacitors, it is well known that the energy density (E) is related to the gravimetric or volumetric cell capacitance (C) and operation voltage (V), i.e.,

$$\mathbf{E} = \frac{1}{2}\mathbf{C}\mathbf{V}^2 \quad (1)$$

And the maximum power density P is determined by

$$\boldsymbol{P} = \frac{\boldsymbol{V}^2}{4*\boldsymbol{ESR}} \quad (2)$$

where ESR is the gravimetric or volumetric equivalent series resistance of the supercapacitor cell.[12] Equation (1) and (2) indicate that the most effective way to increase both power and energy densities is to raise the cell voltage. In general, the operation voltage of supercapacitors is limited by the electrochemical window (ECW) of the electrolyte which is determined by both the electrolyte and the electrode materials.[13] One promising approach to increase the operation voltage and hence the energy and power densities is to assemble asymmetric supercapacitors that make full use of different electrochemical windows of the positive and negative electrodes to increase the maximum cell operation voltage in the devices.[8, 9, 13-16]

Indeed, as demonstarted in the paper, an asymmetric supercapacitor, exploiting an ultra-high density nano-porous aligned activated graphene (a-graphene) flakes as the positive electrode, and nm-scale conformal coating of a conducting polymer, poly(ethylenedioxythiophene) (PEDOT) on aligned carbon nanotubes (A-CNTs) as the negative electrode, is introduced (See Figure 1(a)). The asymmetric configuration of the supercapacitor allows both electrodes to be separately tailored, increasing the device operation voltage and capacitance, leading to power and energy densities beyond all other such carbon-based supercapacitor architectures to date. The a-graphene flakes electrode, fabricated via a self-assembly process, shows high specific gravimetric and volumetric capacitance for the positive electrode. The conformal vapor deposited conducting polymer coating enhances the charge storage of the negative electrode, while the underlying aligned nanowire morphology provides direct non-tortuous fast ion transport pathways to enhance power. As a result of complementary tailoring of the asymmetric electrodes, the layered device exhibits a wide 4V electrochemical window, higher than the individual electrodes, i.e., 2.8 V for PEDOT/A-CNT and 3.2 V for a-graphene. The highest power and energy densities are reported thus far for carbon-based supercapacitors, 149 kW L^{-1} and 113 Wh L^{-1} in volumetric performance and 233 kW kg^{-1} and 177 Wh kg^{-1} in gravimetric performance, respectively. Further enhancement of such devices is

suggested based on the insights developed herein on the tailoring of the nano-morphology and composition of the electrodes.

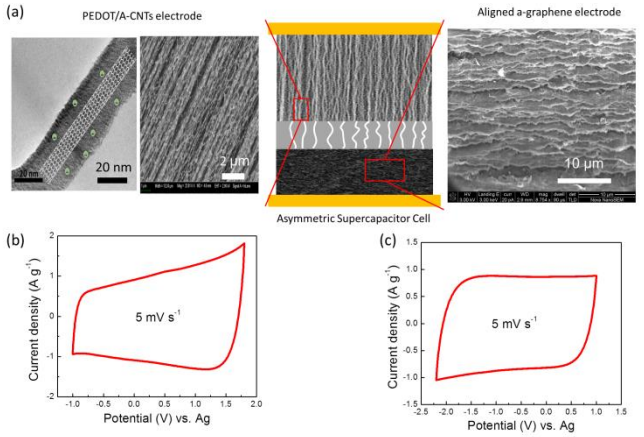

Figure 1. Nanostructured electrodes in asymmetric supercapacitors (a) (left) Low and high magnification TEM micrographs of the negative electrode (negative ions are shown schematically in the PEDOT layer), comprised of conformal oCVD PEDOT on A-CNTs, and (right) SEM images of a-graphene electrode. (b) CV curves of PEDOT/A-CNTs and (c) CV curves of a-graphene at 5 mV s^{-1} in 2 M $BMIBF_4$/PC.

The electrochemical performance of the activated graphene (a-graphene) electrode was characterized using a screen-printed electrode system (Dropsens) with the a-graphene and a Pt current collector as the working electrode, using Ag and Pt as the reference and counter electrodes, respectively. Figure 1(c) presents a CV curve of the a-graphene electrode with 2 M $BMIBF_4$/PC as the electrolyte at a scan rate of 5 mV s-1 showing an ECW of -2.2 V to +1 V. The electrochemical performance of PEDOT/A-CNTs was evaluated by cyclic voltammetry (CV) and galvanostatic charge-discharge tests using a screen-printed electrode system (Dropsens) with the PEDOT/A-CNTs and a Pt current collector as the working electrode, using Ag and Pt as the reference and counter electrodes, respectively. Figure 1 (b) presents a CV curve of the PEDOT/A-CNTs electrode in 2 M $BMIBF_4$/PC at a scan rate of 5 mV s-1, which shows an ECW of -1 V to +1.8 V, indicating that the active material is suitable for the negative electrode. As a result, the asymmetric supercapacitor has a 4 volts (=2.2+1.8) operating voltage, compared with less than 3.5 V for the individual carbon based electrodes.

Due to their favorable ECWs, carbon based electrodes such as activated carbon have been used for the positive electrode in the asymmetric supercapacitors.[1, 8, 14, 17, 18] To significantly improve the capacitance of the positive electrode in this study, a new class of carbon material, the a-graphene was selected due to its superior gravimetric surface area. The a-graphene, first reported by Zhu et al, exhibited a very large specific gravimetric surface area (~ 3100 m^2 g^{-1}) with nano-sized pores and demonstrated a very high gravimetric capacitances of 200 F g^{-1} for supercapacitors.[19] However, the simple mechanical packing of the a-graphene flakes caused a low density (~ 0.3 g cm^{-3}), compared with the graphite density of 2.2 g cm^{-3}, resulting in a low volumetric efficiency of supercapacitors with lower volumetric capacitance of 60 F cm^{-3}.[20] When randomly packing these a-graphene flakes, it is inevitable to remain micron-sized pores in the electrodes, reducing the density. Here, by employing a vacuum assisted self-assembly process,[21, 22] which enabled a-graphene flakes aligned in parallel and stacked successively on top of each other shown in the SEM image of Figure 1(a), the electrode density can be increased markedly to 1.15 g cm^{-3} while preserving the nanoporous morphology of each a-graphene flake. To our knowledge, the density of 1.15 g cm^{-3} of the a-graphene electrode fabricated here is among the highest for the carbon electrodes reported.[23] For example, activated carbon power electrodes fabricated using conventional pressure packing methods have a density of 0.5 g cm^{-3}.[24]

The electrochemical performance of the a-graphene electrode was characterized in detail. The galvanostatic cycles for the electrode at 2 A g^{-1} are presented in Figure 2(a). The symmetric and linear charge and discharge characteristics reveal a rapid I-V response and reversible electrochemical reaction, resulting in an excellent capacitive behavior. The capacitance of the electrode was determined from:

$$\mathbf{C = I/(dV/dt)} \quad (3)$$

where I is the constant current, V is the voltage, and t is time. A high specific volumetric capacitance of 189.7 F cm^{-3} (165 F g^{-1} for gravimetric capacitance) was obtained at 2 A g^{-1}. The high volumetric capacitance performance results from the stacked graphene sheets at a density of 1.15 g cm^{-3}.The a-graphene electrode exhibits high specific capacitance shown in Figure 2(b), ranging from 214.3 F cm^{-3} to 170.4 F cm^{-3} (186.4 F g^{-1} to 148.2 F g^{-1}, Fig S1) as the discharge current increases from 0.5 A g^{-1} to 10 A g^{-1}.

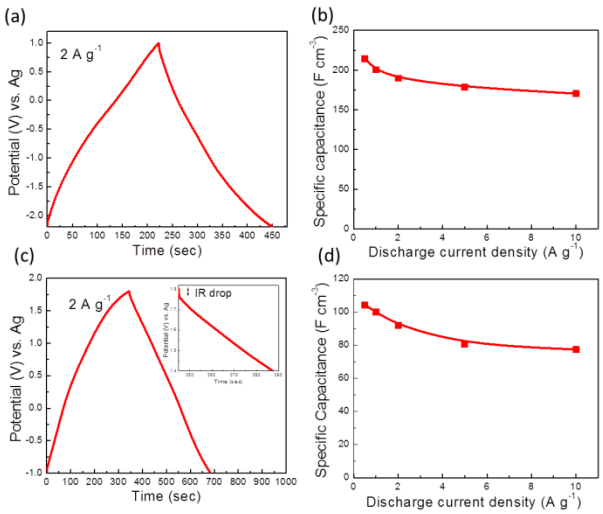

Figure 2. Performance of negative electrode (PEDOT/A-CNTs) and positive electrode (a-graphene) performance. (a) Galvanostatic charge/discharge curves of a-graphene at a current density of 2 A g^{-1}. (b) Specific capacitance at different discharge densities of a-graphene electrode.(c) Galvanostatic charge/discharge curves of PEDOT/A-CNTs composite a current density of 2 A g^{-1}. (d) Specific capacitance at different discharge densities of PEDOT/A-CNTs electrode.

In supercapacitors based on the pure electric double layers, charge storage is limited to the surface of the porous electrode.[17] In contrast, redox reactions occur throughout the entire volume of conducting polymers (CP), allowing for significantly higher energy storage capability. However, CP electrodes typically suffer poor mechanical stability due to volume changes during the doping/dedoping process, which causes mechanical failure of the electrode during long cycling. The composite approach, in which CP layers are deposited on conductive porous networks such as CNTs, can lead to supercapacitors with significantly improved cycling stability.[25, 26] In such a conductive composite approach, the CNT networks provide electron transport pathways as well as mechanical support to the CP while the deposited CP layers enhance the charge storage capacity of the electrodes.[27] The density of A-CNTs is raised by 5 times via a

mechanical densification process to form the scaffold support for the CP coating layer in supercapacitors, and is distinctly advantageous relative to randomly packed morphologies.[28] Apart from the direct ion transport to reduce ESR, as illustrated in Figure 1(a), the PEDOT/A-CNTs also provide better mechanical stability and hence higher retention of the capacitance after long charge/discharge cycles, compared with the electrodes of the PEDOT/randomly packed CNT networks. In the extant literature, electrodes of CP/CNTs were fabricated by electrochemical deposition methods, which will result in non-uniform CP layers on random morphologies of CNTs.[27, 29] In Figure 1(a), the thin (~10 nm) PEDOT layers are deposited as a conformal coating on the very high aspect ratio (~ 10,000) A-CNTs.[30] In order to achieve high volumetric performance of the device, the PEDOT/A-CNT forests were mechanically densified to 5% Vf of A-CNTs.[31]

For the PEDOT/A-CNTs electrode, the slope of the discharge curve in Figure 2(c) (Equation (3)) yields a specific volumetric capacitance of 92 F cm^{-3} at 2 A g^{-1} (230 F g^{-1} for gravimetric capacitance). Figure 2(d) presents the specific volumetric capacitance at different discharge current density, from 0.5 A g^{-1} to 10 A g^{-1}. Capacitance retention of 74.2% was obtained from 104.3 F cm^{-3} at 0.5 A g^{-1} to 77.4 F cm^{-3} at 10 A g^{-1} (260.8 F g^{-1} to 193.5 F g^{-1}, Figure S2), indicating that the PEDOT/A-CNTs electrode provides reliable capacitive performance for high-power applications. This relatively high retention mechanistically arises from the conformal coating of oxidative chemical vapor deposition (oCVD) PEDOT on A-CNTs. The cycling stability of the PEDOT/A-CNTs electrodes was characterized and compared with that of the electrodes of PEDOT deposited on randomly packed CNT networks. As shown in the Supporting Information (Figure S3), symmetric supercapacitors made of the PEDOT/A-CNTs had a retention of 89% after 1000 cycles of 2 V voltage cycle, compared with a retention of 73% after 1000 cycles from PEDOT on random CNT morphologies. At lower voltage of 1 V, the retention of the PEDOT/A-CNTs was increased to 94% while that of the PEDOT on random CNT networks was at 88%. In the randomly packed CNT networks, there are CP layers in the gaps between CNTs and after long charge/discharge cycles, the mechanical failure of CP layers in these gaps will cause disruption of the electric conduction paths between CNTs and reduce the conductivity of CNT networks. As a result, the capacitance is reduced. By contrast, the electric conduction path of the continuous aligned CNTs would not be disrupted by the mechanical failure of the CP coating layers due to the A-CNT/CP foam-like morphology of nm-scale conformal coatings on A-CNTs separated by ~10 nm gaps where ions can move in and out of the CP film. Hence, the A-PEDOT/A-CNTs electrodes exhibit more robust mechanical stability and high retention of the capacitance, compared with the electrodes of the CP deposited on randomly packed CNT networks.

Both electrodes are independently tailored in asymmetric supercapacitors to operate under more optimal conditions. Here, the PEDOT/A-CNTs negative electrode and a-graphene positive electrode were assembled, separated by a 40 μm thick porous paper. 2 M $BMIBF_4$/PC was used as the electrolyte due to its high ionic conductivity.[32] By properly tuning the mass ratio of the two electrodes, the asymmetric capacitor can be operated at the full 4 V cell operation voltage (1.8 V for the negative electrode plus 2.2 V for the positive electrode).[5, 8, 33] From the consideration that charge stored at the two capacitor electrodes should be equal in magnitude with opposite sign and the stored charge q at the electrode is, $q=C\Delta Vm$,where C is the specific gravimetric capacitance, ΔV is the maximum potential range allowed by the ECW, and m is the mass of the electrode, the mass ratio between the two electrodes can be determined by,

$$\frac{m_+}{m_-} = \frac{C_-\Delta V_-}{C_+\Delta V_+} \quad (4)$$

From the specific capacitances of the positive and negative electrodes, 230 F g^{-1} and 165 F g^{-1}, respectively, at a constant discharge current of 2 A g^{-1}, and ΔV_+=1.8 V and ΔV_- =-2.2 V, Equation (4) yields the mass ratio (m_+/m_-) of 0.88.

Figure 3(a) presents the CV curves of the fabricated asymmetric supercapacitors at scan rates from 5 to 100 mV s^{-1} using the 2 M $BMIBF_4$/PC as electrolyte. The capacitors display near rectangular CV curves, especially for the lower scan rates. The galvanostatic cycles at alternate charge/discharge current densities of 2 A g^{-1} and –2 A g^{-1} were presented in Figure 3(b), from which the cell capacitance was determined (Equation (3)). Figure 3(c) presents the cell volumetric capacitances at different discharge currents. It should be noted that the calculated cell capacitance was based on the total volume of positive and negative electrodes because it is not meaningful to deduce the specific capacitance of a single electrode for the asymmetric supercapacitor. Cell volumetric capacitance is obtained as 52.3 F cm^{-3} (81.6 F g^{-1} for gravimetric capacitance, Figure S4) at 0.2 A g^{-1} which is higher than that of a-graphene based symmetric supercapacitors and other conducting polymer based asymmetric supercapacitors.[19, 34] The cell volumetric capacitance using 1 M Et_4NBF_4/PC as electrolyte is exhibited in Figure S5. It can be found that the capacitance with 27.82 F cm^{-3} at 0.2 A g^{-1} which is lower than that of the cell with ILs under 4 V. According our earlier study, the operation voltage will also influence capacitance because higher voltage will result in more diffusion which will increase the cell capacitance.[35] Cycling stability of the asymmetric supercapacitors was demonstrated by continuously cycling the galvanostatic charge/discharge process between 0 and 4 V at a current density of 5 A g^{-1} for more than 5,000 cycles. As shown in Figure 3 (d), the asymmetric supercapacitor maintains electrochemical retention of 92% after 5,000 cycles. The small cell capacitance loss is attributable to the PEDOT/A-CNTs electrode as presented in Figure S3.

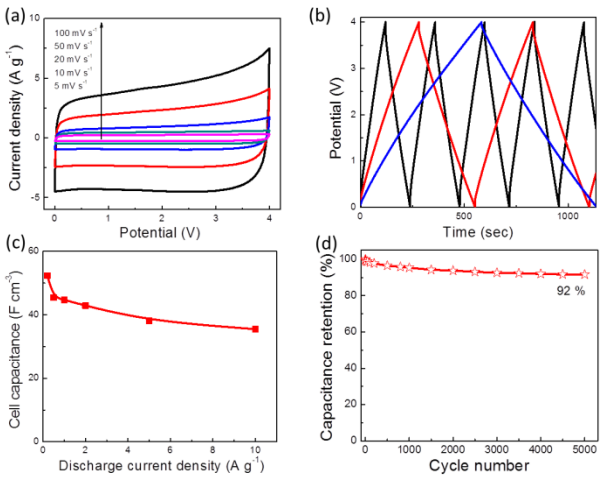

Figure 3. Asymmetric supercapacitor performance (a) CV curves of PEDOT/A-CNTs//a-graphene asymmetric supercapacitor at different scan rates of 5, 10, 20, 50 and 100 mV s^{-1} between 0 and 4 V in 2 M $BMIBF_4$/PC electrolyte. (b) Galvanostatic charge/discharge curves of asymmetric device at a current density of 2, 1 and 0.5 A g^{-1} in black, red and blue, respectively. (c) Cell capacitances of asymmetric cell at different discharge current densities. (d) Cycle capacitance retention of the asymmetric supercapacitor under a voltage of 4 V at a current density of 5 A g^{-1} in 2 M $BMIBF_4$/PC electrolyte.

The electrochemical performance of the asymmetric supercapacitor cell was further characterized by electrochemical

impedance spectroscopy (EIS). Figure S6 shows the Nyquist plot obtained in the frequency range of 100 kHz to 10 mHz of 5 mV applied voltage, which shows a semicircle in the high frequency region and a sharp rise of the imaginary part of the electric impedance, reflecting the dominance of the cell capacitance in the low frequency region. The semicircle in the Nyquist is attributed to the charge transfer resistance of the porous electrodes. The high frequency intersection of the semicircle on the real axis of the Nyquist plot represents the internal resistances including Ohmic resistance of the electrolyte, the resistance of the electrode materials, and resistance in the separator, and the contact resistances between active materials and current collector.[7] The cell shows an internal resistance of 0.1 Ω cm2 when normalized with the area of the current collector of the capacitors, indicating a high electrical conductivity and low ESR of the cells.[12]

The power density of the asymmetric capacitors was determined from Equation (2). The ESR in Equation (2) can be deduced from the data in Figure 2(c),

$$\boldsymbol{ESR} = \Delta \boldsymbol{V}/\Delta \boldsymbol{I} \quad (5)$$

where $\Delta \boldsymbol{V}$ is the voltage change as the current is switched from a positive value to a negative value in Figure 2(c).[12] $\Delta \boldsymbol{I}$ is the current density change between the charge and discharge processes. The linear and small initial resistance (IR) drops with current density even at a high operation voltage (see Figure S7) indicating high-power performance.

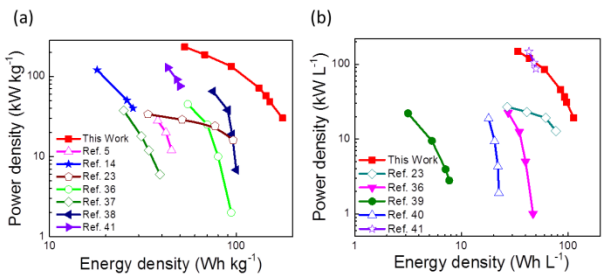

Figure 4. Absolute and relative electrochemical performance of asymmetric cell. (a) Gravimetric and (b) Volumetric Ragone plot of PEDOT/A-CNTs//a-graphene asymmetric supercapacitor cell as compared to the extant literature.

Figure 4(a) and 4(b) present comparative Ragone plots of asymmetric cells in terms of the gravimetric and volumetric performance derived from the galvanostatic discharge curves measured at different charge/discharge current densities. The cells exhibit both high volumetric and gravimetric power and energy densities at 149 kW L^{-1} (233 kW kg^{-1}) and 113.2 Wh L^{-1} (176.6 Wh kg^{-1}), respectively. The Ragone plot of the cell at an operating voltage of 3 V with 1 M Et_4NBF_4/PC is shown in Figure S5 where the energy and power densities are reduced due to the lower EC window. The values under 4V are significantly higher than those of other reported carbon based symmetric supercapacitors, conducting polymer based supercapacitors and other devices reported previously as compared in Figure 4(a) and 4(b).[5, 8, 14, 17, 21, 36-41] All data presented in Fig. 4(a) and Fig. 4(b) as well as Fig. S4, including the references cited, are derived based on the volume/mass of the electrode materials. When using the whole electrode volume/mass, which also include the mass of the electrolyte, the volumetric power and energy densities do not change while the gravimetric power and energy densities become 122 kW kg^{-1} and 92.3 Wh kg^{-1}, respectively, which are still very high due to the high density of the electrode materials.

Conclusions

An asymmetric supercapacitor, exploiting the conformal coating of PEDOT on A-CNTs as the negative electrode which combines fast ion transport pathways, enhances charge storage capability, and reduces ESR, and the a-graphene as positive electrode fabricated from a self-assembly process which possesses exceedingly high specific gravimetric and volumetric capacitance, has been developed in this paper. The positive and negative electrodes materials are individually tailored to control spacing and alignment of graphene and CNTs, and work synergistically together in the asymmetric cell configuration by expanding the ECW. The unique nanomorphology of the conformal coating of CP on A-CNTs also imparts mechanical stability and high cycle retention of the capacitors, compared with electrodes comprised of CP deposited on randomly packed CNT networks. Tailoring of the positive and negative electrode materials at a scale approaching that of the ions can allow asymmetric supercapacitor performance to be further expanded, e.g., utilizing other conducting polymers besides the PEDOT demonstrated here, and further optimizing A-CNT and a-graphene packing densities to expand cell performance further and meet the requirement of a broad range of energy storage applications.

Experimental

Fabrication of a-graphene Electrode

A vacuum-assisted self-assembly method was used to fabricate the highly aligned a-graphene sheets with a high density of 1.15 g cm^{-3}. In this vacuum-assisted self-assembly process, the a-graphene was first dispersed in N,N-dimethylformamide (DMF, Aldrich). [41] Then, this mixture was vacuum filtered using a Buckner funnel and an Anodisc filter paper (Whatman) in order to align a-graphene sheets. During this filtration process, a-graphene flakes are pulled towards the Anodisc surface and these layers of nano-porous graphene stack successively on top of each other.[21] The oriented a-graphene disk was air dried for 2 hours and vacuum dried at 70 ^oC for 1 hour. A commercially available 60 wt% dispersion of PTFE in water (Aldrich) was used to prepare the positive electrode containing PTFE as the binder. The PTFE dispersion was diluted further to 0.6 wt% using isopropyl alcohol (Aldrich). The a-graphene disk was placed in a petri dish containing PTFE dispersion thus prepared. By slowly evaporating water/isopropyl alcohol over one week to ensure uniform distribution of the PTFE, the a-graphene electrode containing 10 wt% PTFE binder was formed. These electrodes were then annealed at 140 ^oC and kept in a dry box for further testing. The thickness of a-graphene electrode is 100 μm.

Conformal coating of PEDOT on A-CNTs

The A-CNTs in this study were grown by a modified CVD method.[31] These as-grown carbon nantotubes (CNTs) have a highly aligned structure with approximately 1% volume fraction and densities of 10^9-10^{10} CNTs per cm^2 and with the tube length of 200 μm. The average diameter of these CNTs is about 8 nm.[42] In the deposition process, the A-CNT arrays were held facing the oxidizing agent in a vacuum chamber. Heating the oxidizing agent allowed for its sublimation into the CNT arrays. EDOT was polymerized using iron chloride as the oxidant. Further reaction of the oxidizing agent with the EDOT monomer resulted in the formation of PEDOT film on the A-CNTs substrates. All PEDOT deposition experiments were performed at a substrate temperature of 70 ^oC and at a pressure of 50 mTorr. TEM images taken from different sections of A-CNTs show that PEDOT was deposited on the surface of all A-CNTs. The coating of PEDOT layer does not affect the electronic conductivity of A-CNTs because there are no chemical reactions between the two layers during the deposition. The thickness of the PEDOT/A-CNT electrode is 200 μm and the PEDOT layer thickness is 10 nm measured by TEM.

Asymmetric supercapacitors and their characterization

PEDOT/A-CNTs and a-graphene electrodes were attached on Au sheets that serve as the current collectors. The asymmetric supercapacitors were prepared by assembling PEDOT/A-CNTs as the negative electrode and self-assembled a-graphene as the positive electrode, which were separated by a porous paper with the thickness of 40 μm. A 2 M $BMIBF_4$/propylene carbonate (PC) mixed electrolyte was used for the asymmetric supercapacitor. For the $BMIBF_4$/PC mixture, 2M $BMIBF_4$/PC exhibits the highest ionic conductivity and hence was chosen for this study.[33] Each electrode was characterized using screen-printed electrodes system (Dropsens) where the PEDOT/A-CNTs or PEDOT/A-CNTs on the platinum current collector for the working electrode, while the silver and platinum were used as the reference and counter electrodes, respectively. For supercapacitor devices, the electrical impedance and CV curves were characterized using a potentiostat/frequency analyzer (Parstat2273). Galvanostatic cycling was measured at different discharge current densities with Versastat 4 (Princeton Applied Research)

Acknowledgements

This work was supported by AFOSR under Grant No. FA9550-11-1-0192 (Penn State and MIT). The authors thank Minren Lin for assistances in the experiment and preparation of the paper. At MIT, this work was performed in part at: the Center for Nanoscale Systems (CNS), a member of the National Nanotechnology Infrastructure Network (NNIN), which is supported by the National Science Foundation under NSF award no. ECS-0335765. and made use of the MIT MRSEC Shared Experimental Facilities supported by the National Science Foundation under award number DMR-0819762, utilized the core facilities at the Institute for Soldier Nanotechnologies at MIT, supported in part by the U.S. Army Research Office under contract W911NF-07-D-0004, and was carried out in part through the use of MIT's Microsystems Technology Laboratories.

Notes and references

[a]Department of Electrical Engineering, [c]Departments of Materials Science and Engineering, [f]Bioengineering and Chemical Engineering Pennsylvania State University, University Park, Pennsylvania 16802 (USA). E-mail: qxz1@psu.edu

[b]Department of Aeronautics and Astronautics, [e]Department of Chemical Engineering, Massachusetts Institute of Technology, Cambridge, MA 02139 (USA). E-mail: wardle@mit.edu

[c]School of Urban Development and Environmental Engineering, Shanghai Second Polytechnic University, Shanghai 201209 (China).

† Electronic Supplementary Information (ESI) available: additional data of electrochemical performance of each electrode and cell. See DOI: 10.1039/c000000x/

1 P. Simon, Y. Gogotsi, *Nat. Mater*. 2008, **7**, 845.
2 B. Chu, X. Zhou, K. Ren, B. Neese, M. Lin, Q. Wang, F. Bauer, Q. M. Zhang, *Science* 2006, **313**, 334.
3 A. Burke, *Electrochim. Acta* 2007, **53**, 1083.
4 J. R. Miller, P. Simon, *Science* 2008, 321, 651.
5 B. G. Choi, M. Yang, W. H. Hong, J. W. Choi, Y. S. Huh, *ACS Nano* 2012, **6**, 4020.
6 C. Liu, F. Li, L.-P. Ma, H.-M. Cheng, *Adv. Mater.* 2010, **22**, E28.
7 B. E. Conway, Electrochemical supercapacitors : scientific fundamentals and technological applications, Kluwer Academic, Plenum Publishers, New York [u.a.] 1999.
8 Z. Fan, J. Yan, T. Wei, L. Zhi, G. Ning, T. Li, F. Wei, *Adv. Funct. Mater.* 2011, **21**, 2366.
9 Z. Tang, C. Tang, H. Gong, *Adv. Funct. Mater.* 2012.
10 A. Janes, H. Kurig, E. Lust, *Carbon* 2007, **45**, 1226.
11 T. Brousse, P. L. Taberna, O. Crosnier, R. Dugas, P. Guillemet, Y. Scudeller, Y. Zhou, F. Favier, D. Belanger, P. Simon, *J. Power Sources* 2007, **173**, 633.
12 P. L. Taberna, P. Simon, J. F. Fauvarque, *J. Electrochem. Soc.* 2003, **150**, A292.
13 V. Khomenko, E. Raymundo-Pinero, F. Béguin, *J. Power Sources* 2006, **153**, 183.
14 P. C. Chen, G. Shen, Y. Shi, H. Chen, C. Zhou, *ACS Nano* 2010, **4**, 4403.
15 Z. S. Wu, W. Ren, D. W. Wang, F. Li, B. Liu, H. M. Cheng, *ACS Nano* 2010, **4**, 5835.
16 K. S. Ryu, Y. G. Lee, Y. S. Hong, Y. J. Park, X. Wu, K. M. Kim, M. G. Kang, N. G. Park, S. H. Chang, *Electrochim. Acta* 2004, **50**, 843.
17 G. A. Snook, P. Kao, A. S. Best, J. Power Sources 2011, 196, 1.
18 X. Huang, Z. Zheng, Z. Fan, J. Liu, H. Zhang, *Adv. Mater.* 2012, **24**, 5979.
19 Y. Zhu, S. Murali, M. D. Stoller, K. Ganesh, W. Cai, P. J. Ferreira, A. Pirkle, R. M. Wallace, K. A. Cychosz, M. Thommes, D. Su, E. A. Stach, R. S. Ruoff, *Science* 2011, **332**, 1537.
20 Y. Gogotsi, P. Simon, *Science* 2011, **334**, 917.
21 Q. Liang, X. Yao, W. Wang, Y. Liu, C. P. Wong, *ACS Nano* 2011, **5**, 2392.
22 K. W. Putz, O. C. Compton, C. Segar, Z. An, S. T. Nguyen, L. C. Brinson, *ACS Nano* 2011, **5**, 6601.
23 X. Yang, C. Cheng, Y. Wang, L. Qiu, D. Li, *Science* 2013, **341**, 534.
24 K. Miura, H. Nakagawa, H. Okamoto, Carbon 2000, **38**, 119.
25 H. Lee, H. Kim, M. S. Cho, J. Choi, Y. Lee, *Electrochim. Acta* 2011, **56**, 7460.
26 L. Chen, C. Yuan, H. Dou, B. Gao, S. Chen, X. Zhang, *Electrochim. Acta* 2009, **54**, 2335.
27 V. Gupta, N. Miura, *Electrochim. Acta* 2006, **52**, 1721.
28 C. Peng, S. Zhang, D. Jewell, G. Z. Chen, *Prog. Nat. Sci.* 2008, **18**, 777.
29 V. Gupta, N. Miura, *J. Power Sources* 2006, **157**, 616.
30 S. Vaddiraju, H. Cebeci, K. K. Gleason, B. L. Wardle, *Acs Appl. Mater. Interfaces* 2009, **1**, 2565.
31 B. L. Wardle, D. S. Saito, E. J. Garcia, A. J. Hart, R. G. de Villoria, E. A. Verploegen, *Adv. Mater.* 2008, **20**, 2707.
32 T. Nishida, Y. Tashiro, M. Yamamoto, *J. Fluor. Chem.* 2003, **120**, 135.
33 X. Lu, M, Yu, G. Wang, T. Zhai, S. Xie, Y. Ling, Y. Tong, Y. Li, *Adv. Mater.* 2013, **25**, 267.
34 K. Machida, S. Suematsu, S. Ishimoto, K. Tamamitsu, *J. Electrochem. Soc.* 2008, **155**, A970.
35 J. Lin, Y. Liu, Q. Zhang, Polymer 2011, 52, 540.
36 A. Izadi-Najafabadi, S. Yasuda, K. Kobashi, T. Yamada, D. N. Futaba, H. Hatori, M. Yumura, S. Iijima, K. Hata, *Adv. Mater.* 2010, **22**, E235.
37 Z.-L. Wang, R. Guo, L.-X. Ding, Y.-X. Tong, G.-R. Li, *Sci. Rep.* 2013, **3**, 1204.
38 M. Zhi, A. Manivannan, F. Meng, N. Wu, *J. Power Sources* 2012, **208**, 345.
39 E. Raymundo-Piñero, M. Cadek, M. Wachtler, F. Béguin, *ChemSusChem* 2011, **4**, 943.

40 Z. Chen, J. Wen, C. Yan, L. Rice, H. Sohn, M. Shen, M. Cai, B. Dunn, Y. Lu, *Adv. Energy Mater.* 2011, **1**, 551.
41 M. Ghaffari, Y. Zhou, H. Xu, M. Lin, T. Y. Kim, R. S. Ruoff, Q. M. Zhang, *Adv. Mater.* 2013, **25**, 4879.
42 Y. Zhou, M. Ghaffari, M. Lin, E. M. Parsons, Y. Liu, B. L. Wardle, Q. M. Zhang, *Electrochim. Acta* 2013, **111**, 608.